Journal of Engineering Science and Technology
Vol. 19, No. 1 (2024) 246 - 275

ADVANCEMENTS IN ADDITIVE MANUFACTURING: INNOVATIONS IN DIRECT INK WRITING MATERIALS AND THEIR TRANSFORMATIVE PRACTICAL APPLICATIONS

S. SIVARAO[1], K. Y. SARA LEE[2], K. KUMARAN[3,*], D. RAMASAMY[4], A. M. KASSIM[5], M. S. SALLEH[1], U. K. VATESH[6], S. PUJARI[7], R. DHARSYANTH[8]

[1] Faculty of Industrial and Manufacturing Engineering and Technology, Universiti Teknikal Malaysia Melaka, 76100 Durian Tunggal, Melaka, Malaysia
[2]Center of Systematic Innovation Research, Department of Mechanical Engineering, Faculty of Engineering and Technology, Tunku Abdul Rahman University of Management and Technology, 53300 Kuala Lumpur, Malaysia
[3]Faculty of Mechanical and Automotive Engineering Technology, Universiti Malaysia Pahang Al-Sultan Abdullah, 26600 Pekan, Pahang, Malaysia
[4]Faculty of Mechanical Engineering, College of Engineering, Universiti Malaysia Pahang Al-Sultan Abdullah, 26300, Gambang, Pahang, Malaysia
[5]Faculty of Electrical Technology and Engineering, Universiti Teknikal Malaysia Melaka, 76100 Durian Tunggal, Melaka, Malaysia
[6]Mechanical Engineering Department, Amity University, 201301, Uttar Pradesh, Noida, India
[7]Lendi Institute of Engineering and Technology, Vizianagaram, 535005, Andhra Pradesh, India
[8] Faculty of Industrial and Manufacturing Engineering and Technology, Universiti Teknikal Malaysia Melaka, 76100 Durian Tunggal, Melaka, Malaysia
*Corresponding Author: kumaran@umpsa.edu.my

Abstract

The domain of three-dimensional (3D) printing holds limitless potential, encompassing a diverse range of materials and applications. This review offers a comprehensive exploration of the Direct Ink Writing (DIW) technique within additive manufacturing, alongside recent breakthroughs in material advancement. The purview extends to encompass DIW methodologies, graphene oxide, hydrogels, shape-memory polymers, ceramics, polymers, and composite-based materials. The discussion delves into the multifaceted potential of 3D printing materials and their prospective applications, notably emphasizing the transformative role of DIW. The versatility of DIW is showcased in various fields, including energy storage, electronics, soft robotics, and biomedical applications. Through an in-depth analysis of capabilities of DIW and the diverse materials it encompasses, this review sheds light on the promising avenues that lie ahead in the evolving landscape of additive manufacturing.

Keywords: Direct ink writing, Graphene oxide, Robocasting, Shape-memory polymers, Three-dimensional (3D) printing.

1. Introduction

Conventional manufacturing is characterized by high energy consumption and environmental pollution. Additive manufacturing, particularly the Direct Ink Writing (DIW) technique, offers a solution to create more sustainable industries. DIW, which is also known as Direct Write Fabrication, Robocasting, or Robot-Assisted Shape Deposition, falls within the classification of material extrusion methods [1]. Initially developed by Cesarani et al. in 1997 at Sandia National Laboratories, DIW was designed for producing concentrated materials, like ceramic pastes with organic binders. This simple, versatile, and cost-effective technology can be applied to various materials such as metals, ceramics, composites, and polymers [1]. In its ambient state, DIW printing material presents as a non-Newtonian viscous slurry comprising both liquid and solid phases [2]. One of its key advantages lies in its ability to fabricate parts without the need for machining or moulds, thus minimizing emissions and raw material consumption. The extrusion process allows for the use of water-based inks, contributing to reduced energy usage. The adaptability of DIW encompasses a broad spectrum of materials, including metals, highlighting its versatility [3].

The DIW process is executed through computer-controlled robots manoeuvring dispensers filled with printing ink. This ink is extruded under pressure through micronozzles to build up layer-by-layer geometries, enabling high printing resolution [4]. Notably, DIW demonstrates superiority over alternative printing techniques due to its minimal raw material usage, capacity for multi-material printing, broad material options, and open-source nature [5]. The technique is particularly suitable for lab settings and excels in printing nanocomposites featuring transparent or opaque nanoparticles.

DIW techniques can be categorized into two approaches which are droplet-based and filamentary (continuous) inks as illustrated in Fig. 1. These inks are commonly composed of colloidal, polymeric, or polyelectrolyte building blocks, which are either suspended or dissolved in a liquid or heated to achieve a stable, homogeneous ink with the desired and reproducible rheological (or flow) behaviour [6]. The success of DIW hinges on precise control of ink viscosity, which is influenced by rheological parameters [7]. These parameters include viscoelastic characteristics, shear yield strength, shear loss, and apparent viscosity [6]. Shear-thinning behaviour pertains to a condition where viscosity diminishes as shear forces within the nozzle intensify - this phenomenon is of paramount importance during the DIW fabrication process [8].

Shear-thinning facilitates the extrusion of inks under pressure through fine or micronozzles. Subsequent to ink discharge from the nozzle, both shear yield strength and high shear elastic modulus regain their original values. This deposition process preserves the intended shape, maintaining a filamentary structure on both sides, which is essential for the step-by-step layering process. Ensuring the proper viscosity is a prerequisite for successful DIW. This can be achieved by regulating printing temperature and introducing additives to manage rheological characteristics, thereby ensuring effective control for successful printing endeavours [9, 10].

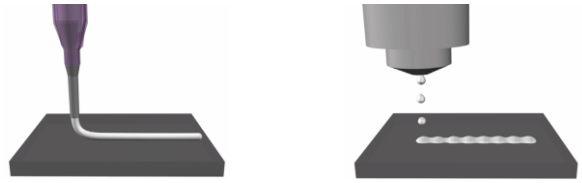

(a) droplet-based inks. **(b) filamentary-based inks.**

Fig. 1. Illustrative representation of ink-based deposition methods [6].

While the exploration of multi-material printing is in its initial research phases, its potential for substantial influence in fields like electronics and biomedical is noteworthy. The integration of diverse materials within a single manufacturing procedure not only diminishes assembly duration but also minimizes waste [11]. This integration holds the promise of introducing novel structural and functional products, encompassing composites and gadgets. Notably, among additive manufacturing techniques, material extrusion and material jetting stand out as the sole methods exhibiting potential in the domain of multi-material printing [12]. This study is dedicated to delving into the different materials, applications, limitations and challenges associated with DIW.

2.Materials

In this study, DIW emerges as the focal technology under thorough exploration, primarily owing to its extensive potential with graphene oxide, shape-memory polymers, hydrogels, ceramics, polymer and composites-based materials. The distinctive viscoelastic attributes inherent to these materials render them extensively applicable in the fabrication of three-dimensional (3D) and four-dimensional (4D) parts [13].

2.1. Graphene oxide-based materials

Graphene-based inks play a pivotal role in enhancing the efficacy of 3D printing applications [14]. Given that DIW relies on the rheology of the suspension, precision in determining the optimal component concentration becomes imperative. DIW was leveraged for fabricating composites using graphene-infused ceramic pastes, thereby facilitating an investigation into product quality and mechanical attributes [12].

2.1.1. Graphene-reinforced resin for biotissue generation

An intriguing insight emerged, highlighting that graphene-reinforced resin possesses a higher potential for generating biotissues compared to conventional mould-based procedures. Within the domain of DIW rheological assessments, two key effects surfaced: the shear-thinning (pseudoplastic) behaviour was consistent across all studied pastes, and the concentration of Graphene Oxide (GO) wielded a notable influence on viscosity. Specifically, the 5 wt.% GO-alumina composite demonstrated the highest apparent viscosity, as shown in Fig. 2. The yield stress of the ink containing 5 wt.% of GO content exhibited a notably higher value compared to the inks with different compositions. When the GO content ranged from 0 to 5 wt.%, the yield stress values escalated from 20 to 220 Pa, respectively. On

comparative analysis, DIW has demonstrated the capability to improve the mechanical properties of graphene composites [15].

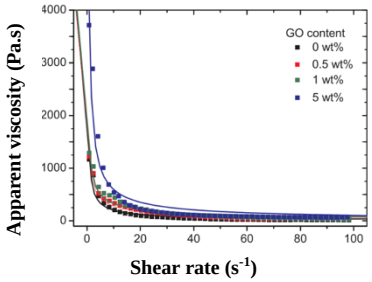

Fig. 2. Relationship between apparent viscosity and shear rate for inks containing varying amounts (0, 0.5, 1, 5 wt.%) of GO in GO-alumina composites [15].

2.1.2. Graphene in flexible electronics

The combination of remarkable electrical attributes alongside the inherent flexibility of graphene serves as a compelling catalyst for the utilization of graphene inks within the realm of flexible electronic circuitry. A study investigated on the resistance variation with bending cycles for graphene lines on PEN (Teonex Q51, 50 µm) after inkjet printing with Intense Pulsed Light (IPL) annealing at 5.6 and 7.8 J.cm^{-2}. The resistance of these circuits showcased remarkable resilience, enduring more than 1000 bending cycles with the bending radii of curvature of 8.1 mm, across a spectrum of energy densities as shown in Fig. 3 [16].

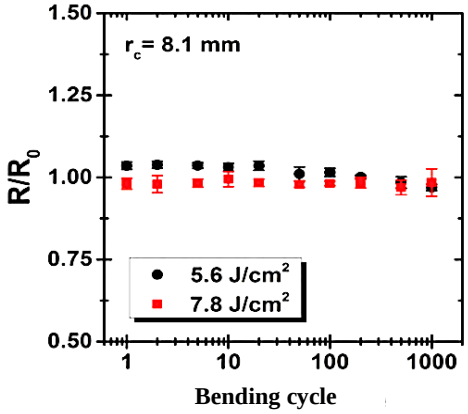

Fig. 3. Variation in resistance with bending cycles for graphene patterns on PEN after IPL annealing at 5.6 and 7.8 J.cm^{-2}, utilizing bending radii of 8.1 mm [16].

The study emphasized the allure of graphene as a viable material for printed electronics. It presents a chemically stable, mechanically pliable, and electrically conductive substitute, offering advantages over traditional metal nanoparticle and conductive polymer inks [16]. Another study highlights that the inherent flow behaviour of liquid crystals GO fundamentally differs from that commonly

observed in viscoelastic materials, including polymers. Even at higher concentrations (up to 13.35 mg.ml^{-1}), there was an absence of the elastic storage and viscous loss moduli (*G′–G″*) crossover phenomenon within the frequency range under investigation, up to 100 Hz. In addition, the observed behaviour resembled that of a gel-like substance, akin to cells or soft glassy materials, characterized by an exceptionally high elastic modulus ranging from 350 to 490 Pa [17].

2.1.3. Graphene-based composite electrode and components

A separate study introduces a composite electrode composed of Super-P aerogel and Reduced Graphene Oxide (rGO). This electrode is distinguished by its controllable porous structure, achieved through DIW. The combination of substantial specific area, high conductivity, and a well-organized hierarchical porous arrangement contributes to its exceptional attributes. In Table 1, the cell featuring the optimized Super-P/rGO aerogel electrode showcases a remarkable discharge capacity of 848 mA.h at a current density of 80 mA.cm^{-2}, as compared to other materials. This represents a significant enhancement of 14.9% compared to the performance of cells utilizing the conventional graphite felt electrode, demonstrate promising potential in vanadium redox flow battery [18].

Table 1. Discharge capacity for different materials [18].

	Discharge Capacity (mA.cm^{-2})
Reduced Graphene Oxide (rGO)	715.1
Traditional graphite felt	738.2
Carboxylic multi-walled carbon nanotubes/rGO	759.5
Carbon nanofibers/rGO	761.3
Super-P/rGO	848.4

In a recent investigation, a novel aqueous-phase pristine graphene ink was developed for 3D printing. This ink utilizes a formulation involving a conductive nanofibrillar network, achieved by precisely controlling the interfacial interactions between graphene and Poly (3,4-ethylenedioxythiophene): poly(styrenesulfonate) (PEDOT: PSS) nanofibrils. A set of inks consisting of graphene/PEDOT:PSS, with concentrations ranging from 1 to 9 wt.%, was formulated as shown in Fig. 4. It was found that the thixotropic nature of the inks intensifies with the concentration of graphene/PEDOT:PSS, as the formulated inks progressively transition from fluidic dispersions to 3D printable inks. Figure 5(a) displays the printed filaments of the 5 wt.% ink, exhibiting a smoother texture in contrast to the 7 wt.% ink shown in Fig. 5(b). The precision of printing for the 5 wt.% and 7 wt.% G/PEDOT:PSS inks were determined to be 72% and 96%, respectively [19].

Fig. 4. Images illustrating graphene/PEDOT:PSS inks across varying concentration levels (1, 3, 5, 7, 9 wt.%) [19].

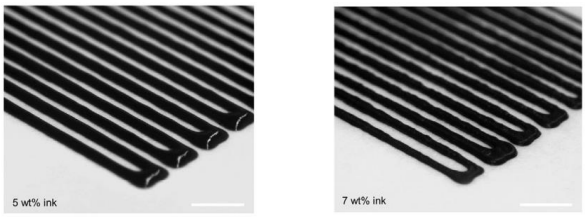

(a) 5 wt.% ink. **(b) 7 wt.% ink.**

Fig. 5. Images of printed filament at different concentration levels of graphene/PEDOT:PSS inks [19].

The shape retention of the formulated inks was also assessed through contact angle measurements of the printed filaments, as illustrated in Fig. 6. At lower concentrations, the contact angle measurement reveals significant lateral spreading of the inks upon deposition on the glass substrate (contact angle of 71° for the 3 wt.% ink), rendering them unsuitable for 3D printing. As graphene/PEDOT:PSS concentrations increase, the printed filaments exhibit reduced spreading and improved shape retention, featuring a distinct ink-substrate interface (contact angles of 107° and 125° for the 5 wt.% and 7 wt.% inks, respectively), indicating their suitability for multilayer printing [19].

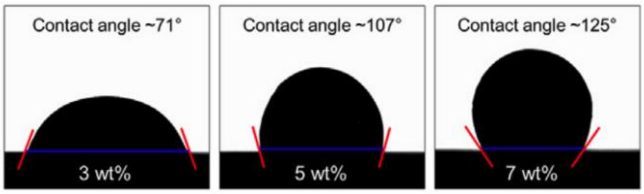

(a) 3 wt.%. **(b) 5 wt.%.** **(c) 7 wt.%**

Fig. 6. Contact angle measurement of the printed filaments at different ink concentrations [19].

In a separate investigation, 3D components were fabricated through the DIW process, utilizing a self-synthesized suspension composed of kaolin and GO composite. As the proportion of GO was augmented, the apparent viscosities and shear elastic/loss moduli of the suspensions exhibited an increase. Notably, the incorporation of GO lamellas led to a significant enhancement in both flexural and compressive strengths when compared to the cured pure kaolin suspension. As shown in Fig. 7, the flexural strength attained its peak value of 8.2 MPa, marking a substantial 63% increase compared to the reference samples. Likewise, the compressive strength achieved its maximum value of 39.5 MPa, showcasing a remarkable 72% enhancement relative to the comparison samples [20].

Table 2 provides a succinct summary of diverse materials explored in the context of DIW with a focus on graphene oxide-based compositions. The GO-alumina composite demonstrates tuneable viscosity, while graphene on PEN displays remarkable durability with over 1000 bending cycles. The Super-P/rGO composite electrode outperforms in discharge capacity, and kaolin/GO composites

reveal enhanced mechanical strengths, showcasing the versatility and promise of DIW in graphene-based applications.

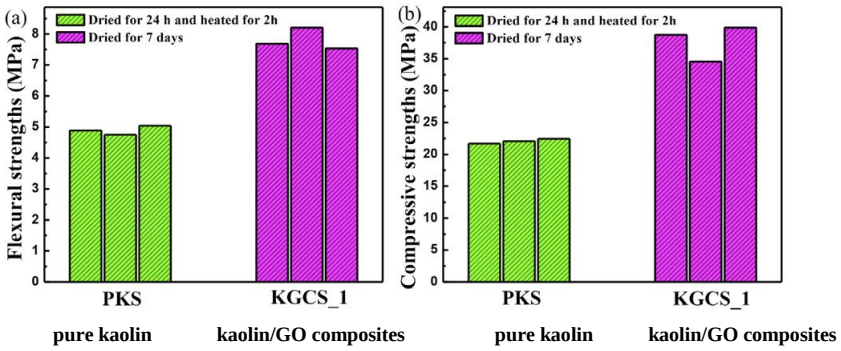

(a) flexural strength. **(b) compressive strength.**

Fig. 7. Mechanical characteristics of pure kaolin and kaolin/GO composites under various curing conditions [20].

Table 2. Summary of DIW-printed graphene oxide-based materials.

Material	Composition/ Process	Key Findings
GO-alumina composite	0, 0.5, 1, 5 wt.% of GO	The 5 wt.% GO-alumina composite demonstrates the highest apparent viscosity [15].
Graphene on PEN	IPL annealing at 5.6 and 7.8 J.cm^{-2}	Remarkable resilience with more than 1000 bending cycles, even at small radii of curvature (8.1 mm) [16].
Super-P/rGO Composite	rGO, Traditional graphite felt, Carboxylic multi-walled carbon nanotubes/rGO, Carbon nanofibers/rGO, Super-P/rGO	Super-P/rGO aerogel electrode showcases a remarkable discharge capacity of 848 mA.h at 80 mA.cm^{-2}, 14.9% enhancement compared to other materials [18].
Graphene/PEDOT:PSS	1, 3, 5, 7, 9 wt.% of PEDOT:PSS	The 7 wt.% samples exhibit 96% printing precision and contact angle of 125°, suitable for multilayer printing [19].
Kaolin/GO composite	Pure kaolin, kaolin/ GO composites	Kaolin/GO composites yielded peak flexural strength at 8.2 MPa (63% increase), maximum compressive strength at 39.5 MPa (72% enhancement) compared to pure kaolin [20].

2.2. Shape memory polymers (SMPs)

While graphene-based materials exhibit remarkable versatility, ranging from biotissue generation to flexible electronics, Shape Memory Polymers (SMPs) introduce a dynamic dimension to the DIW landscape. SMPs are recognized as the prototypical materials for 4D printing owing to their distinctive property. This property allows 4D printed SMP objects to undergo deformation in response to

external stimuli, diverging from the static state characteristic of traditional 3D printing. As a result, the dominance of 4D printing using SMPs becomes evident over 3D printing with conventional polymers, particularly in the domain of shape-changing materials. The application of various SMPs in 4D printing using DIW is evident, encompassing materials such as polyurethane (PU) [21, 22], polylactic acid (PLA) [23], epoxy [24], polycaprolactone (PCL) and others [25].

The conventional heat-activated shape memory test consists of a sequential procedure comprising four distinct stages. To commence, the sample undergoes heating above its transition temperature, which can be exemplified by the glass transition temperature (T_g). During this stage, the sample experiences deformation under the influence of an external load. Subsequently, the deformation is sustained while the temperature is lowered below the T_g. In the third step, the external force is eliminated, leading to the fixation of the temporary shape of the sample. Finally, the sample undergoes reheating to reach the T_g once more, thereby causing it to revert back to its initial shape [24]. For SMPs, shape fixity (R_f) and shape recovery (R_r) ratio values were calculated from Eq. (1) and (2), respectively:

$$R_f = \frac{\varepsilon}{\varepsilon_{load}} \times 100\% \quad (1)$$

$$R_r = \frac{\varepsilon - \varepsilon_{rec}}{\varepsilon_{rec}} \times 100\% \quad (2)$$

where ε_{load}, ε, *and* ε_{rec} denote the strain before unloading, the strain after unloading, and the strain after recovery for a shape, respectively. The values of ε_{rec} and ε were based on the termination point of the strain plateau in the recovery curve [25].

2.2.1. Semicrystalline PCL

A study conducted research to showcase the development of a flexible shape memory through DIW additive manufacturing. This was achieved by utilizing semicrystalline PCL as the base material, along with a photoinitiator, a diacrylate cross-linker, a rheology modifier, and n-butyl acrylate monomer to formulate a solvent-free printing ink. The ink was subjected to a temperature of 70°C to disrupt PCL crystallization and enable smooth extrusion. Each printed pattern was then cross-linked using ultraviolet (UV) light. The effect of DIW-printed elastomeric tube is illustrated in Fig. 8, from initial shape, fixed temporary shape, and recovered initial shape [25].

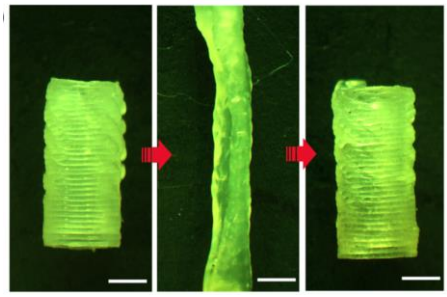

(a) **(b)** **(c)**

Fig. 8. Shape memory effect of a DIW-printed elastomeric tube, with a scale bar of 2 mm, (a) initial shape, (b) fixed temporary shape, and (c) recovered initial shape [25].

As in Fig. 9(a), under stress-controlled testing mode with a programming strain exceeding 230%, the first cycle exhibited a shape fixity surpassing 93%, accompanied by a shape recovery ratio exceeding 95%. Alternatively, under strain-controlled testing mode (with a stretching strain of 200%), the shape fixity reached approximately 99% over four cycles (Fig. 9(b)), while the shape recovery ratio showed a gradual decrease from 90% to 83% across the same cycles. The semicrystalline PCL network also contributed to a fracture strain of 500–600% at different printing angles from 0, 45 to 90° [25].

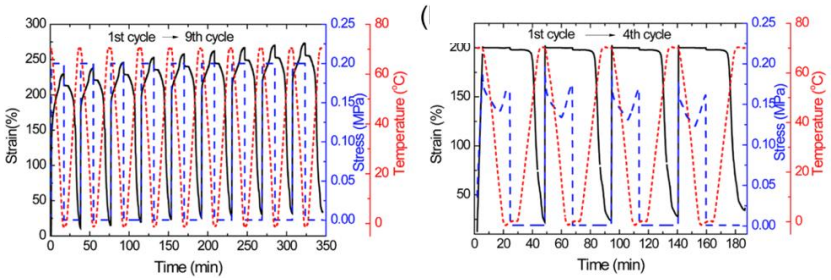

(a) stress-controlled mode. **(b) strain-controlled mode.**

Fig. 9. Stress-strain behaviour of printed semi-IPN elastomers that examined using stress and strain-controlled modes [25].

2.2.2. Tracheal scaffold design with PLA and PCL composites

Utilizing the capabilities of 4D printing, a technique that employs intelligent materials for 3D printing, researchers successfully harnessed the attributes of SMPs to manufacture a tracheal scaffold as in Fig. 10 [23, 26]. In a particular study, varying compositions of PLA and PCL composites were subjected to 4D printing utilizing the DIW technique. In this context, PLA was employed as a stable phase responsible for maintaining the initial shape of sample, while PCL served as a reversible phase, aiding in the transition to and fixation of a temporary shape. By incorporating PCL into the composite, the flexibility of the samples was notably improved, allowing them to maintain their temporary shape following deformation. Concurrently, the T_g of the blends exhibited a decrease from 61 to 49°C with an increasing proportion of PCL within the PLA/PCL blend. Notably in Table 3, the PLA70/PCL30 blend demonstrated an optimal combination of and recovery and shape fixity, with ratio of 90-91% [23].

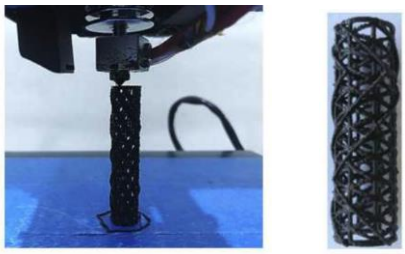

(a) **(b)**

Fig. 10. 4D printed tracheal scaffold using the shape memory PLA/iron oxide composite, (a) 4D printing process, (b) tracheal scaffold [26].

Table 3. Shape fixity and shape recovery ratios for printed PLA/PCL strips [23].

Material	Shape fixity ratio (%)	Shape recovery ratio (%)
PLA	76	97
PLA70/PCL30	91	90
PLA50/PCL50	94	79
PLA30/PCL70	98	74

2.2.3. UV-responsive SMP composites

In a recent study, a novel approach involved the creation of ultraviolet light responsive SMP composites through the application of DIW 3D printing. This method integrated shape memory polyurethane (PU) with laboratory-prepared lignin nanotubes (LNT) to serve as UV absorbents. The resulting 3D printed LNT/PU composite demonstrated an impressive shape recovery ratio of 99% when exposed to UV radiation at a wavelength of 370 nm for a duration of 15 minutes as shown in Table 4. Furthermore, the tensile strength of the 3D printed SMP composite with 5wt.% LNT, experienced a substantial enhancement to 16.4 MPa, signifying a remarkable 131% increase over that of the pristine PU material, which possessed a tensile strength of 7.11 MPa. Notably, the T_g of the 3D printed LNT/PU SMP composite displayed a gradual shift from 47 to 33°C upon elevating the content of LNT to 9%. This adjustment contributes to the enhanced potential application versatility of the resulting composites [27].

Table 4. Shape fixity and recovery rate for printed LNT/PU SMP composites [27].

Material	Shape fixity ratio (%)	Shape recovery ratio (%)	Tensile Strength (MPa)
PU	97.9	6.2	7.11
PU/1wt.% LNT	98.2	92.5	11
PU/3wt.% LNT	98.6	95.6	15
PU/5wt.% LNT	98.7	98.2	16.4
PU/7wt.% LNT	99.1	98.4	10
PU/9wt.% LNT	98.8	98.1	8

In a conducted study, UV-assisted DIW-printed thermally cured epoxy composites demonstrated notable characteristics, including elevated tensile toughness and favourable shape memory effects. The utilization of Interpenetrating Polymer Network (IPN) epoxy composites resulted in the enhancement of tensile toughness while offering the flexibility to adjust mechanical properties. Specifically, the moduli values were reported as 1.31, 1.06, and 0.61 GPa for weight fractions of 20, 30, and 40% photopolymer, respectively. Furthermore, the ultimate strain values were measured at 13.7, 18.1, and 32.1% for the respective weight fractions. The T_g of the composites exhibited tunability, spanning from 7 to 95°C. Notably, the shape fixity ratio stood at approximately 97%, while the shape recovery ratio was approximately 98.5% [24].

Table 5 provides a concise summary of shape fixity and recovery rates for SMPs. Notably, PU/5wt.% LNT SMPs emerge as the most promising, showcasing a remarkable shape fixity and recovery ratio exceeding 98%, coupled with a high tensile strength of 16.4 MPa. Besides, the IPN epoxy composites demonstrated notable attributes, including a shape fixity of 97%, shape recovery of 98.5%, and tuneable mechanical properties.

Table 5. Summary shape fixity and recovery rate for SMPs.

Material	Shape fixity ratio (%)	Shape recovery ratio (%)	Key Findings
Semicrystalline PCL	> 93	> 95	PCL demonstrated fracture strain of 500–600% [25].
PLA	76	97	PLA70/PCL30 blend demonstrated an optimal combination of and recovery and shape fixity, with ratio of 90-91% [23].
PLA70/PCL30	91	90	
PLA50/PCL50	94	79	
PLA30/PCL70	98	74	
PU	97.9	6.2	
PU/1wt.% LNT	98.2	92.5	PU/5wt.% LNT experienced a substantial tensile strength of 16.4 MPa [27].
PU/3wt.% LNT	98.6	95.6	
PU/5wt.% LNT	98.7	98.2	
PU/7wt.% LNT	99.1	98.4	
PU/9wt.% LNT	98.8	98.1	
IPN epoxy composites	97	98.5	Tuneable mechanical properties and favourable shape memory effects [24].

2.3. Hydrogels

SMPs exhibit impressive shape-shifting abilities, while DIW in hydrogels has attracted considerable attention for their versatility and biocompatibility. This attention stems from DIW's capacity to craft intricate, complex, and remarkably adaptable structures under ambient conditions. These structures find application across a wide array of domains, notably within the biomedical, flexible electronics, or other sectors [28, 29]. Hydrogels represent a category of polymeric 3D structures adept at both retaining and dispensing substantial volumes of water or biological fluids, often exceeding their dry weight by thousands of times. Characterized by their adaptable mechanical attributes, notable porosity, and pliant texture, hydrogels hold remarkable versatility as biomaterials in diverse biomedical contexts [30, 31].

2.3.1. Plant-based bio-hydrogels

Of particular importance are hydrogels originating from natural sources, commonly referred to as bio-hydrogels, primarily derived from plant materials. These bio-hydrogels have gained increasing attention due to their inherent benefits, such as biocompatibility and hydrophilicity. Employing the DIW method, a succession of 3D bio-hydrogels composed of 2,2,6,6-tetramethylpiperidin-1-oxy-oxidized cellulose nanofibrils and aloe vera gel were successfully fabricated. Moreover, assessment of physical and structural attributes of the 3D-printed specimens was conducted, revealing their compliance with preliminary prerequisites for the envisaged applications. An example of a flower pattern created using DIW is also presented in Fig. 11. All the examined samples exhibited notable characteristics, including a high porosity exceeding 80%, along with remarkable water uptake capacity and retention ability [28].

Fig. 11. A demonstration of a flower pattern created through DIW printing using aloe vera/cellulose nanofibrils bio-hydrogel ink [28].

2.3.2. Carbomer as a rheology modifier

A study introduces a novel 3D printing technique that leverages the rheology-modifying agent Carbomer for the DIW of various hydrogels with specific functions. This research reveals Carbomer's remarkable efficacy in achieving desirable rheological characteristics for multifunctional hydrogel inks. Notably, these inks encompass various types of hydrogels, such as biogels, magnetic hydrogels, temperature-sensitive hydrogels, and double network hydrogels. The introduction of Carbomer at low concentrations (starting from 0.5% w/v), is demonstrated to yield optimal results.

The study further uncovers that the incorporation of Carbomer contributes to enhancing the mechanical characteristics of hydrogels. This enhancement is attributed to the interaction between the polymeric matrix of the hydrogel and the polymeric chains of Carbomer. The investigation showcases an increase in Young's modulus, rising from 17 to 40 kPa, while concurrently noting a reduction in critical stretch from 547 to 260% as the Carbomer concentration escalates from 0.5 to 5.0% w/v, as shown in Fig. 12 [32].

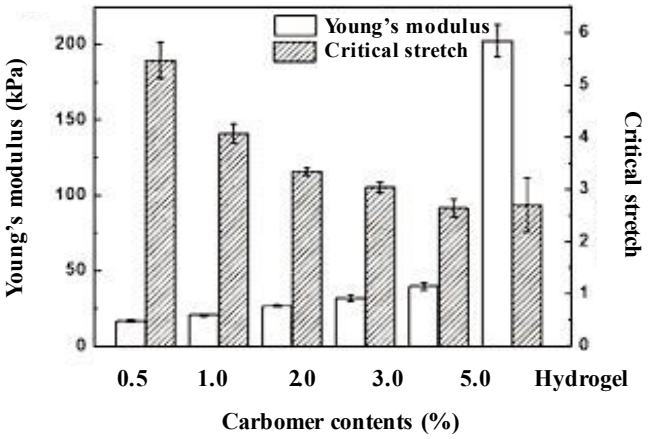

Fig. 12. Effect of carbomer's content on Young's modulus and stretchability of hydrogels [32].

2.3.3. 'Living' hydrogel photoinks

In a recent study, a novel type of hydrogel photoinks was developed, known as "living" hydrogel photoinks (Fig. 13), which utilized the mechanism of reversible addition/fragmentation chain transfer polymerization involving type I photoinitiation. These specialized hydrogel photoinks were specifically formulated for utilization in DIW 3D printers. The unique property of "livingness" was effectively demonstrated by generating 3D printed parent hydrogel objects using a single-material approach. This achievement was facilitated by implementing post-production modification of photoiniferter with N,N-dimethyl acrylamide and N-isopropyl acrylamide, showcasing the distinctiveness of the concept [33].

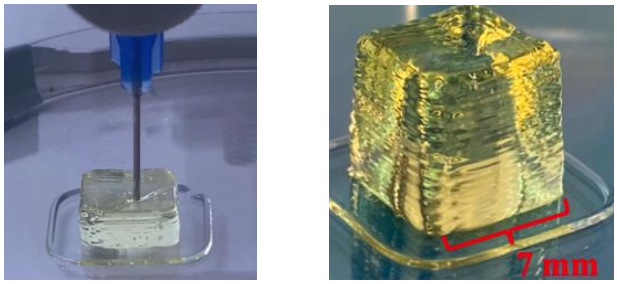

(a) **(b)**

Fig. 13. (a) The extrusion of "living" photoink in the DIW printing process and (b) a “living” printed hydrogel cube [33].

2.4. Ceramics based-materials

A research study introduces an additive manufacturing investigation focused on a ceramic paste tailored for DIW applications within the ceramic industry. The study involved the formulation of several compositions featuring varying volumetric ratios of solids to water, spanning from 50 to 56%. To enhance the paste's properties, two distinct additives which are sodium polyacrylate and sodium silicate were incorporated at concentrations ranging from 0.2 to 0.8 wt.%. The resulting printable components were selected based on their capability to maintain their shape throughout the printing process, subsequent sintering, and suitability for diverse applications such as flooring and bathroom materials, tableware, and structural components [1, 14].

2.4.1. Alumina

Cesarano et al. [34] who are credited with pioneering the robocasting technique, introduced the use of DIW technology to fabricate alumina components. In their seminal study, the slurry formulation exhibited a significant solid loading (exceeding 60 vol.%) while incorporating a minimal quantity of organic binder less than 1 vol.%. In a study, ceramic on-demand extrusion approach was introduced. The formulation comprised 60 vol.% of alumina powder with methylcellulose, ammonium polymethacrylate and deionized water. The printed alumina had a relative density of 98%, a Young’s modulus of 371 GPa, flexural strength of 364 MPa, a fracture toughness of 4.5 MPa.m$^{1/2}$, and a hardness of 19.8 GPa [35].

A DIW technique was employed to manufacture dense alumina ceramics, utilizing a low organic content (including 0.54 wt.% dispersants and 0.9 wt.% binders) and viscoelastic ink. The resulting printable inks (Fig. 14) exhibited a high-volume fraction of alumina, reaching up to 81 wt.%. Alumina with 1 wt.% of TiO_2 and sintered at 1500°C, exhibit a relative density of 97%, flexural strength measuring 176.5 MPa, and Vickers hardness reaching 15.21 GPa [36]. In another study, highly pure alumina and yttria powders in a percentage–weight ratio of 64:36 was mixed with 0.2 wt.% MgO in a total solid loading of 42 vol% in aqueous media, adding carboxymethyl cellulose and polyethyleneimine solution as additives. Samples sintered at 1600 and 1650°C presented similar average Vickers hardness values of about 14.5 GPa, with a relative density above 95% [37].

Fig. 14. DIW-printed alumina bodies [36].

In a recent investigation, thorough examination has been carried out on the incorporation of nanoparticle effects into the densification and rheological characteristics of inks used in DIW. Initially, aqueous-based alumina-silica inks were formulated, utilizing nano-silica derived from waste rice husk ash at varying proportions (0–10 wt.%). The results revealed a consistent reduction in the solid-to-liquid ratio as nano-silica content increased, thereby impacting the printable rheological properties of the inks. The nano-silica improves the packing efficiency of the system by filling the inter-particle pores, resulting in a decrease in porosity as shown in Fig. 15 [38].

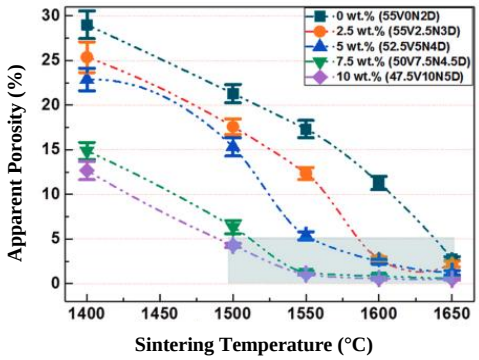

Fig. 15. Effect of apparent porosity in samples with varying amounts of nano-silica sintered at different temperatures [38].

2.4.2. Zirconia

Alumina, with their high-volume fraction and minimal organic content, exemplify the adaptability of DIW in crafting intricate designs. Shifting the lens to zirconia, where studies focusing on tailored slurries for dental components and intricate

structures, underscoring the versatility of DIW in achieving exceptional mechanical properties. A study focused on formulating a high-solid loading slurry (60 vol.%) intended for DIW of yttria-partially-stabilized zirconia. The resulting sintered components displayed an impressive density of 98%. Notably, the research asserted that the fracture toughness, flexural strength, and compressive strength of the produced parts exceeded the performance achieved by alternative manufacturing techniques, including selective laser sintering and binder jetting [39].

Another study employed a slurry with 27 vol.% solid loading to 3D print zirconia dental components. The resulting parts demonstrated exceptional mechanical properties, including a fracture toughness of 6.7 MPa.m$^{1/2}$ and a strength of 763 MPa [40].

In a different study, a research endeavour focused on formulating zirconia slurries with high solid loading (80–90 wt.%) for the purpose of DIW fabrication of molar tooth structures, all without the inclusion of an organic binder. The DIW process utilized a paste consisting of 88 wt.% zirconia and 0.5 wt.% Dolapix CE64 as the dispersant agent.

An example of the molar tooth prototype is shown in Fig. 16. After undergoing the sintering process, the generated samples attained a density of 97% of theoretical density, showcased a fracture toughness of 4.11 MPa.m$^{1/2}$ and Vickers hardness of 1485 HV. These properties closely resembled those observed in parts fabricated using the slip-casting method [41]. Notably, the manufacturing costs of DIW printed zirconia crowns are lower than the manufacturing costs of CAD/CAM-milled crowns [42].

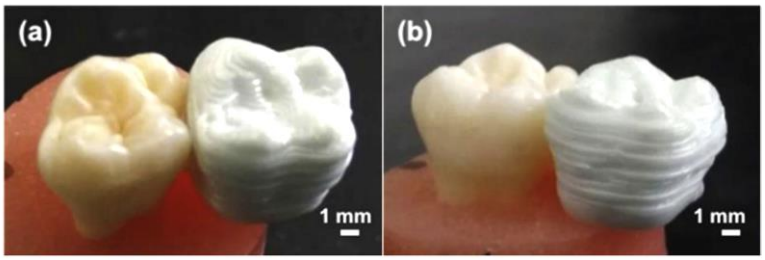

(a) top view. **(b) side view.**

Fig. 16. A prototype of a DIW-printed molar tooth (right side of each photo), with an extracted human molar (left side of each photo) for comparison purposes [41].

Table 6 summarizes the composition or formulation of ceramics-based materials. Alumina materials generally demonstrate relative densities of 95% and above, along with remarkable flexural strength and fracture toughness. Alumina-silica composites, incorporating nano-silica, exhibit improved packing efficiency and reduced porosity. On the other hand, zirconia-based materials generally demonstrate relative densities of 97% and above. The materials also present fracture toughness values varying from 4.11 to 6.7 MPa.m$^{1/2}$. Overall, these materials showcase varying mechanical and structural properties suitable for diverse applications in DIW-based additive manufacturing.

Table 6. Summary of ceramics-based materials.

Material Composition/ Formulation	Key Findings
60 vol.% of alumina powder with methylcellulose, ammonium polymethacrylate and deionized water	Relative density of 98%, Young's modulus of 371 GPa, flexural strength of 364 MPa, fracture toughness of 4.5 MPa.$m^{1/2}$, hardness of 19.8 GPa [35].
81 wt.% alumina and 1 wt.% of TiO_2	Relative density of 97%, flexural strength of 176.5 MPa, Vickers hardness of 15.21 GPa [36].
Alumina-yttria with 0.2 wt.% MgO (solid loading of 42 vol%)	Relative density above 95%, Vickers hardness of 14.5 GPa [37].
Alumina-silica composites with nano-silica derived from waste rice husk ash (0, 2.5, 5, 7.5,10 wt.%)	Nano-silica improves the packing efficiency with a decrease in porosity [38].
60 vol.% of solid loading of yttria-partially-stabilized zirconia.	Relative density of 98% [39].
27 vol.% solid loading of zirconia	Fracture toughness of 6.7 MPa.$m^{1/2}$, strength of 763 MPa [40].
80–90 wt.% solid loading of zirconia	Relative density 97%, fracture toughness of 4.11 MPa.$m^{1/2}$, Vickers hardness of 1485 HV [41].

2.5. Polymer and composites based-materials

While ceramics offer unique properties and applications, the focus now shifts towards the versatility and innovations brought forth by polymers and composites. DIW has found applications in the fabrication of polymer nanocomposites to enhance battery performance. The flexibility of DIW surpasses that of traditional machining methods, making it compatible with a wide range of battery sizes and geometries. Regarding materials, while polyethylene oxide (PEO) has been commonly employed for battery electrolyte fabrication, there is a dearth of studies showcasing DIW's utilization in developing PEO electrolytes [43]. Cheng et al. demonstrated that DIW is viable for printing polymer electrolytes tailored for Li-ion batteries due to their elevated apparent viscosity and viscoelastic properties. Enhanced printing characteristics of PEO polymers were achieved through the functionalization of hexagonal boron nitride with silane, generating silane-hexagonal boron nitride [44].

PEDOT: PSS is a promising conducting polymer although its rheological characteristics are not well-suited for DIW applications. A study sought to address this limitation by leveraging a non-conductive viscoelastic polymer with excellent spinnability, namely PEO. Through this approach, an ideal suspension comprising 52 wt.% PEO and 4.33 wt.% PEDOT: PSS was identified as shown in Fig. 17. This formulation displayed an exceptionally favourable blend of rheological characteristics, encompassing elongational, shear, and thixotropic behaviours. Consequently, the formulation demonstrated exceptional printability and notable filament-shape retention subsequent to the printing process [45].

A recent study introduced an innovative printing approach that utilizes DIW technology to create polymer-derived ceramics reinforced with chopped fibres. This process involves polymer infiltration and pyrolysis (PIP) and aims to produce carbon fibre/silicon carbide (SiC) composites characterized by high strength and

minimal shrinkage. The results of the study demonstrate that the composite with a carbon fibre content of 30 wt.% showcases minimal linear shrinkage (0.5%) and significant bending strength of 7 MPa as shown in Fig. 18(a). Remarkably, after undergoing ten PIP cycles, the bending strength of the composite remarkably increased to approximately 100 MPa (Fig. 18(b)), demonstrating a substantial enhancement of approximately 30 times in comparison to the pure SiC matrix lacking carbon fibre reinforcement [46].

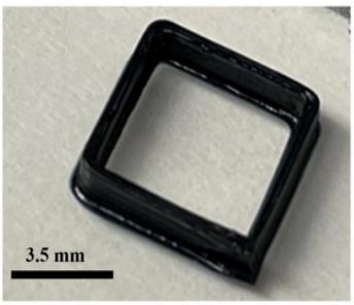

Fig. 17. A DIW-printed structure created using a mixture of 52 wt.% PEO and 4.33 wt.% PEDOT: PSS [45].

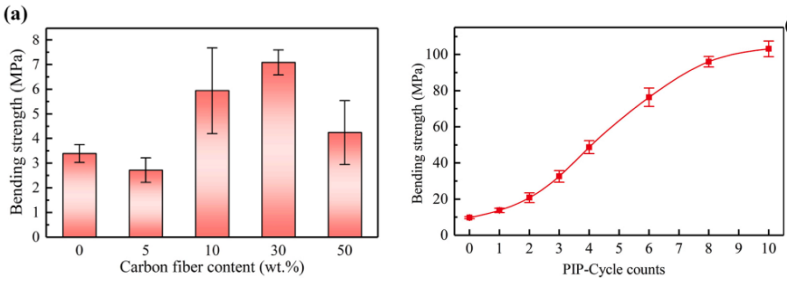

(a) carbon fibre content. **(b) PIP-cycle counts.**

Fig. 18. Effect of carbon fibre content (0, 5, 10, 30, and 50 wt.%) and PIP-cycle counts (0 – 10) on the bending strength of fibre/SiC composites [46].

In summary, graphene-based inks demonstrate exceptional electrical conductivity, making them suitable for electronic applications. SMPs exhibit shape memory effects crucial for dynamic and responsive structures. Hydrogels, derived from natural and synthetic sources, present biocompatibility and hydrophilicity, enhancing their utility in biomedical applications. Ceramics-based materials, including alumina and zirconia formulations, showcase high densities, flexural strengths, and fracture toughness, catering to diverse industrial needs. Polymer-based materials, such as polyethylene oxide (PEO) and PEDOT: PSS, are leveraged for battery electrolytes, demonstrating enhanced printability. The distinctive differences lie in the unique properties each material imparts, from electrical conductivity to shape memory to biocompatibility. Parameters like electrical conductivity, shape fixity and recovery ratios, porosity, and mechanical strength are crucial considerations when selecting materials for DIW, emphasizing the adaptability of the technology to a broad spectrum of applications.

3. Applications

3.1. Electronics and energy storage

DIW is a commonly employed method for the fabrication of various functional electronic components, encompassing transistors, sensors, antennas, and light-emitting diodes. Abas and Rahman [47] adopted a combination of direct writing followed by a packing technique to create sensing arrays using carbon paste inks and carbon nanotube. Subsequently, these arrays were enclosed within photocurable resin and PET, resulting in precisely controlled sensor array shapes that led to reliable sensing outcomes. Consequently, the production of consistent, high-quality soft sensors using printable liquid metals is viable [48].

3.1.1. Mechanochromic sensors

DIW proves to be a promising avenue for generating high-resolution wear sensors, benefiting from its advantageous features. Parekh et al. [49] reported achieving line-to-line spacing and line width as small as 100 μm and 25 μm, respectively, through this technology. Li et al.[50] surpassed this record by achieving a line spacing of 50 μm with 15 μm silver lines, employing a 25 μm nozzle and the appropriate ink selection. Furthermore, studies have explored the effects of printed material surface topography and ink rheology on line resolution in integrated circuits employing DIW [51].

Additionally, Chen et al. [52] developed a precursor ink that was employed through the DIW technique in conjunction with UV curing. This procedure involved the use of polybutylene acrylate spheres and a UV initiator that were expanded through 2-Ethylhexyl acrylate monomers, leading to the formation of a mechanochromic sensor. The subsequent UV light curing of the precursor led to the formation of a photonic crystal hydrogel that exhibited both elasticity and mechanochromic behaviour as show in Fig. 19. Specifically, the hydrogel changed colour as strain increased, providing a visual indication of the applied mechanical stress [52].

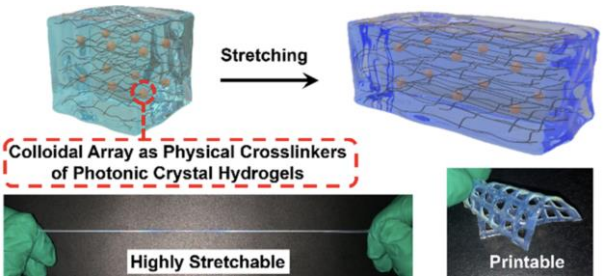

Fig. 19. Highly stretchable photonic crystal hydrogels for a sensitive mechanochromic sensor [52].

3.1.2. Electrochemical energy storage

In a recent study, the hybrid electrode material of silver nanoparticles -MXene (Ag-Ti_3C_2) that fabricated using DIW, demonstrated enhanced supercapacitive performance attributed to its enhanced electrical conductivity and outstanding redox contributions. The asymmetric supercapacitor device was constructed using

DIW-printed Ag-Ti_3C_2 as the anode and printed MnO_2-Ti_3C_2 as the cathode materials. This configuration exhibited a maximum energy density of 38.16 $W.h.kg^{-1}$ along with minimum power density of 800 $W.kg^{-1}$. The results highlighted in this study suggest that the incorporation of hybrid structures introduces novel opportunities for the progression of high-performance printed electrochemical energy storage devices [53].

A separate research initiative demonstrated Li-ion batteries that are both scalable and versatile in shape, fabricated using the DIW printing technique, as shown in Fig. 20. These batteries were coupled with high-performance printable gel polymer electrolytes. This innovative strategy highlights significant potential as a practical solution for supplying power to specific applications as required, showcasing flexible aesthetics, delivering competitive electrochemical performance, and accommodating designs without constraints [54].

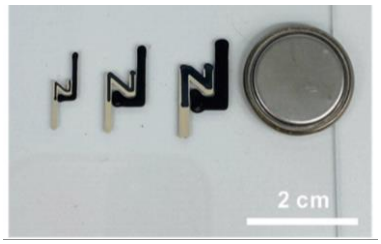

Fig. 20. Three different sizes of scalable DIW-printed anodes and cathodes [54].

3.2. Biomedical

Transitioning from the exploration of electronics and energy storage applications to the biomedical arena, the adaptability of DIW technology becomes even more pronounced. Over the past decade, polymers and ceramics have experienced remarkable growth within the realm of biomedical materials [55]. This surge in popularity can be attributed to the cost-effectiveness and enhanced durability of polymers in comparison to metals. Certain polymers also exhibit attributes such as biocompatibility, elasticity, and bio-inertness. This unique combination of properties inherent to polymeric materials has opened avenues for the creation of tailored structures [56].

3.2.1. Ear tissue and implants

An additional dimension was introduced by Visscher et al. [57], who brought attention to scaffold contraction as a crucial factor to be considered. This becomes particularly significant in practical endeavours such as ear tissue engineering, where achieving optimal mechanical compliance without compromising cell sources and scaffold properties is imperative. Figure 21 shows the side and top views of the PCL cage-like construct. Besides, cage constructs showed no shrinkage or deformation after in vitro culturing. Consequently, the development of a cage-like structure encapsulating materials like PCL emerges as an intriguing facet of ongoing research [57]. Besides, the human ear could be produced via DIW using the Alginate-PCL-HA ink as depicted in Fig. 22 [31].

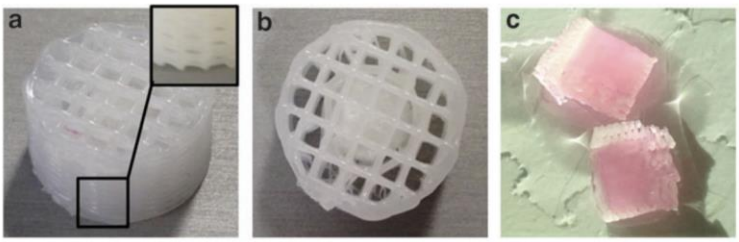

(a) (b) (c)

Fig. 21. PCL cage construct (a) side view, (b) top view, (c) scaffold after in vitro culturing [57].

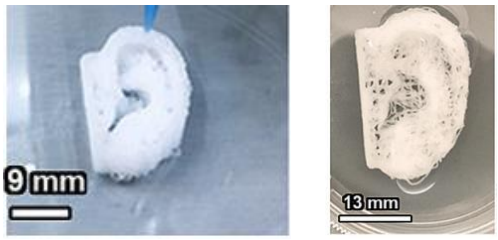

(a) (b)

Fig. 22. Scalable, personalized, and gradient human ear implants DIW-printed using the Alginate-PCL-HA ink [31].

3.2.2. Scaffold engineering for bone tissue

The DIW multi-nozzle forming method offers a distinctive advantage by enabling precise spatial arrangement of desired growth factors, cell numbers, or other bioactive substances compared to conventional forming methods. Yan et al. [58] devised a multi-nozzle system to produce scaffolds and constructs for bone tissue engineering. This approach employed single, double, or triple-nozzle deposition techniques to tailor the characteristics of the produced bone tissue engineering scaffolds.

DIW techniques have gained popularity for the fabrication of hydroxyapatite (HA), zirconia and alumina-based materials in biomedical applications [59-61]. Alumina, a type of ceramic material, showcases remarkable mechanical and physical properties. These include exceptional compressive strength, a high elastic modulus, outstanding resistance to wear and corrosion, and notably resistance to chemical and thermal degradation even under high temperatures [1]. Yttria-tetragonal zirconia polycrystal (Y-TZP) stands out for its impressive mechanical properties. It exhibits fracture toughness range of 4 to 10 MPa.m$^{1/2}$, accompanied by a Young's modulus approximately within the range of 180 to 210 GPa. Additionally, Y-TZP exhibits a notable fracture strength that falls within the range of 900 to 1200 MPa and a Vickers hardness of 11 to 13 GPa [62].

In a study, the DIW method was employed for the fabrication of porous HA scaffolds featuring a bimodal pore structure. The study utilized a concentrated HA ink with a solid loading of 45 vol.%. The research further delved into the in vivo reaction of the HA scaffolds, aiming to gain insight into how the structure of the scaffold influences the growth of bone [63]. By employing a water-based ink with

a concentration of 70 wt.%, the DIW method effectively created 3D cylindrical and woodpile zirconia scaffolds. Microscopic examination revealed the proliferation of HCT116 cells in the vicinity of the zirconia scaffolds. The 3D porous internal structure of these scaffolds proves advantageous for cell growth, offering increased attachment sites and proliferation areas for cells. Remarkably, the woodpile scaffold with around 63% porosity displayed a compressive strength of 8 MPa, whereas the cylindrical scaffold with 55% porosity exhibited an even higher compressive strength of 10 MPa, as shown in Fig. 23. These values notably exceeded the compressive strength of HA scaffolds [64].

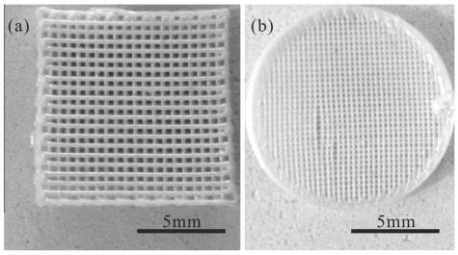

(a) woodpile. (b) cylindrical.

Fig. 23. 3D zirconia scaffolds [64].

Zirconia-toughened alumina (ZTA) materials have also found applications in bone and tissue engineering, utilizing the capabilities of DIW technology. The achievement of shape retention was realized by employing a well-dispersed and stable ink with the solid loading of 70 wt.%, that was injected into an acid pH water bath. The application of DIW-ZTA demonstrated successful culture of human osteoblasts on ZTA scaffolds, with even distribution throughout the entire scaffold thickness [59].

3.3. Soft robotics

The attributes of polymers and ceramics, previously harnessed in biomedical contexts, now manifest in creative ways within the realm of soft robotics, showcasing the extensive versatility of DIW across diverse applications. In recent years, there has been a surge of research interest in soft robotics, driven by its potential to seamlessly integrate motion agility, ensure human interaction safety, and adapt to unstructured environments [65]. An innovative hybrid magnetorheological material is created through the application of DIW, comprising magnetorheological fluid and magnetorheological elastomer [66]. This material demonstrates the robust magnetorheological effect characteristic of magnetorheological fluid and exhibits substantial mechanical stability akin to magnetorheological elastomer Using the DIW 3D printing process, soft robotic grippers are effectively manufactured. Impressively, the magnetorheological material displays superior clamping force (7×10^{-3} N) and swifter response rate (2 seconds) in comparison to alternative actuators. In Fig. 24, the gripper grabs up the PU foam with 6 seconds under 300 mT magnetic field. This study introduces an innovative approach for crafting high-performance hybrid magnetorheological materials, holding significant potential across diverse applications [66].

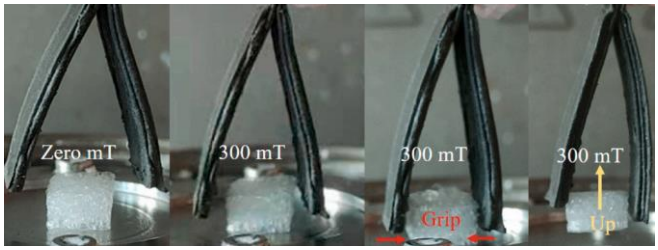

Fig. 24. Gripping process of the magnetorheological gripper [66].

In a more recent study, a multi-material DIW process is utilized to achieve a one-step fabrication method for flexible sensing materials and magnetic soft materials. This process facilitates seamless integration between flexible electronics and magnetic soft robots. The integration design within the multi-material system imparts the robot with seamless incorporation of diverse sensing capabilities, including electrochemical sensing (with a detection limit of 0.036 mM for sodium hydroxide solutions), tactile sensing (such as material recognition), and temperature sensing (with a linearity of 3.383 kΩ/°C). Consequently, the magnetic soft robot proposed in this study, enriched with multifunctional sensing capabilities, has the potential to propel the field of future magnetic soft robot [67].

DIW technology finds diverse applications across various domains, showcasing its adaptability and versatility, as summarized in Table 7. DIW has played a pivotal role in advancing electrochemical energy storage and mechanochromic sensors. In the biomedical field, DIW has demonstrated adaptability in ear tissue engineering and contributed to scaffold engineering for bone tissue applications. DIW has brought about groundbreaking advancements, from crafting hybrid magnetorheological materials for robotic grippers to enabling the one-step fabrication of flexible sensing materials and magnetic soft materials.

Table 7. Applications of DIW technology.

Application	Material	Key Findings
Mechanochromic Sensors	Hydrogel and UV curing	Mechanochromic sensor formed through UV curing of precursor ink, exhibiting colour change with strain [52].
Electrochemical Energy Storage	Silver nanoparticles - MXene (Ag-Ti3C2)	DIW-fabricated hybrid electrode material demonstrated enhanced supercapacitive performance [53, 54].
Biomedical	Alginate-PCL-HA, HA, ZTA	Human ear implants, scaffolds and constructs for bone tissue engineering [31, 64].
Soft Robotics	Magnetorheological fluid, elastomer, various polymers	Soft robotic grippers, flexible sensing and magnetic soft materials in soft robotics [66, 67]

4. Limitations and challenges

4.1. Structural limitations

In the realm of 3D printing, many materials necessitate curing through UV or heat exposure. It's crucial to recognize that each material undergoes different levels of shrinkage or expansion during the curing process. Discrepancies in the shrinkage

strain among various printing materials can lead to complications like warping and bending [68]. The thickness of each printed layer is a fundamental consideration for ensuring quality. An important aspect to note is that increasing the layer thickness can result in inaccurately estimated curvature, leading to a phenomenon known as "stair-stepping," which is an error inherent to the technology [69].

Conventional DIW techniques may present limitations such as poor structural properties. UV-assisted DIW can be implemented, where ceramics are mixed with photopolymers and extruded layer by layer under ultraviolet exposure. This approach enhances the structural integrity of overhangs in scaffolds. While some photopolymers used in this process may be toxic and expensive, the multi-material DIW method offers a solution by allowing the extrusion of two or more materials. This technique is particularly useful for co-extrusion and creating ceramic components with support structures, ultimately improving overall structural properties [60].

4.2. Rheological considerations

Having explored the complexities associated with material shrinkage, layer thickness, and structural integrity, the focus now shifts to the profound influence of rheological properties. The additive manufacturability of ceramic slurries is significantly influenced by their rheological properties. The bottleneck in achieving complex geometries through the DIW process lies in challenges such as clogging of the deposition nozzle and the incapacity of the deposited slurry to support the load of subsequent layers.

Highly viscous slurries encounter consistency issues during the DIW process, leading to prolonged processing times, clogging, and sudden slurry release. These issues constrain the printing time, part conformity, and dimensional accuracy of the DIW process. Addressing this problem involves establishing a correlation between the rheological behaviour of the slurry and its printability [1]. Furthermore, enhanced nozzle designs or nozzle size have the potential to alleviate the choking issue [70].

4.3. Size scaling considerations

Negotiating challenges posed by highly viscous slurries, clogging issues, and the delicate balance of consistency in the DIW process, the transition into size scaling becomes imperative. Achieving defect-free parts with uniform and isotropic properties on a large scale, both in terms of quantity and size, continues to be a significant challenge in ceramic 3D printing [71]. Moreover, when contemplating DIW processing models, it is essential to thoroughly address the size scale of the process. Models tailored for concrete printing, involving 1–10 mm beads, may not be applicable to parts featuring 100–500 μm beads. Small-scale components are affected by factors that may be disregarded on a larger scale, such as surface tension [72]. On the contrary, the timescales for the cooling or evaporation of large parts are considerably longer than those for small parts [73].

DIW technology confronts a spectrum of challenges, including structural limitations such as variations in shrinkage and layer thickness that impact print quality. While UV-assisted DIW offers some solutions, concerns persist regarding the toxicity of photopolymers. Rheological issues, including slurry consistency and

nozzle clogging, pose obstacles to efficient printing. Potential mitigations involve the implementation of enhanced nozzle designs and size adjustments. The process of size scaling introduces complexities in achieving uniform large-scale parts, necessitating considerations for bead size and timescales. Addressing these challenges is imperative to enhance the broader applicability of DIW across diverse industries.

5. Conclusions

The review has highlighted the boundless potential inherent in 3D printing. A comprehensive perspective has been provided on the significant role of DIW within the additive manufacturing landscape, along with recent advancements in material exploration. The array of additive manufacturing methods spans various materials, including graphene oxide, hydrogels, shape-memory polymers, polymers, ceramics, and composite-based materials. Additionally, the discourse has delved into the extensive array of materials achievable through DIW printing, shedding light on promising avenues for applications. DIW emerges as a prominent candidate capable of ushering in transformations in fields such as electronics, energy storage, biomedical applications, and soft robotics. The limitations and challenges in ceramic 3D printing encompass a spectrum of factors that directly influence structural integrity, rheological considerations, and size scaling. By channelling efforts towards overcoming structural, rheological, and size scaling challenges, the future of DIW could witness transformative breakthroughs, leading to broader applications and enhanced capabilities in the realm of 3D and 4D printing.

Acknowledgement

The authors sincerely acknowledge the unwavering support and invaluable contributions of the Faculty of Industrial and Manufacturing Technology and Engineering, Universiti Teknikal Malaysia Melaka and the Ministry of Higher Education Malaysia. Their support and resources have been instrumental in the successful completion of this critical review, revealing the advancements in the field of 3D printing. The authors would also like to extend their gratitude to all individuals who have provided their expertise, data, and assistance throughout the research process. Their contributions have greatly enriched the outcomes of this study to be further connected with the research grants at both University and Ministry levels.

Nomenclatures

G'	Elastic Storage Moduli
G''	Viscous Loss Moduli
R_f	Shape Fixity Ratio
R_r	Shape Recovery Ratio
T_g	Glass Transition Temperature

Abbreviations

3D	Three-Dimensional
4D	Four-Dimensional
DIW	Direct Ink Writing

GO	Graphene Oxide
HA	Hydroxyapatite
IPL	Inkjet Printing with Intense Pulsed Light
IPN	Interpenetrating Polymer Network
LNT	Lignin Nanotubes
PCL	Polycaprolactone
PEDOT:PSS	Poly(3,4-Ethylenedioxythiophene): Poly(Styrenesulfonate)
PEO	Polyethylene Oxide
PIP	Polymer Infiltration and Pyrolysis
PLA	Polylactic Acid
PU	Polyurethane
RGO	Reduced Graphene Oxide
SiC	Silicon Carbide
SLA	Stereolithography
SMPs	Shape Memory Polymers
UV	Ultraviolet
Y-TZP	Yttria-Tetragonal Zirconia Polycrystal
ZTA	Zirconia-Toughened Alumina

References

1. Shahzad, A.; and Lazoglu, I. (2021). Direct ink writing (DIW) of structural and functional ceramics: recent achievements and future challenges. *Composites Part B: Engineering*, 225(1), 109249.
2. Chen, Z.; Li, Z.; Li, J.; Liu, C.; Lao, C.; Fu, Y.; Liu, C.; Li, Y.; Wang, P.; and He, Y. (2019). 3D printing of ceramics: a review. *Journal of the European Ceramic Society*, 39(4), 661-687.
3. Altıparmak, S.C.; Yardley, V.A.; Shi, Z.; and Lin, J. (2022). Extrusion-based additive manufacturing technologies: state of the art and future perspectives. *Journal of Manufacturing Processes*, 83(1), 607-636.
4. Hou, Z.; Lu, H.; Li, Y.; Yang, L.; and Gao, Y. (2021). Direct ink writing of materials for electronics-related applications: a mini review. *Frontiers in Materials*, 8(1), 1-8.
5. Nazir, A.; Gokcekaya, O.; Masum, B.K.; Ertugrul, O.; Jiang, J.; Sun, J.; and Hussain, S. (2023). Multi-material additive manufacturing: a systematic review of design, properties, applications, challenges, and 3D printing of materials and cellular metamaterials. *Materials & Design*, 226(1), 111661.
6. Lewis, J.A.; and Gratson, G.M. (2004). Direct writing in three dimensions. *Materials Today*, 7(7-8), 32-39.
7. Li, L.; Lin, Q.; Tang, M.; Duncan, A.J.E.; and Ke, C. (2019). Advanced polymer designs for direct-ink-write 3D printing. *Chemistry – A European Journal*, 25(46), 10768-10781.
8. Farahani, R.D.; Dubé, M.; and Therriault, D. (2016). Three-dimensional printing of multifunctional nanocomposites: manufacturing techniques and applications. *Advanced Materials*, 28(28), 5794-821.
9. Thibaut, C.; Denneulin, A.; Rolland, S.; Beneventi, D.; Orgéas, L.; and Chaussy, D. (2019). A fibrous cellulose paste formulation to manufacture

structural parts using 3D printing by extrusion. *Carbohydrate Polymers*, 212(1), 119-128.

10. Ovhal, M.M.; Kumar, N.; and Kang, J.W. (2020). 3D direct ink writing fabrication of high-performance all-solid-state micro-supercapacitors. *Molecular Crystals and Liquid Crystals*, 705(1), 105-111.
11. Taneja, H.; Salodkar, S.M.; Parmar, S.A.; and Chaudhary, S. (2022). Hydrogel based 3D printing: bio ink for tissue engineering. *Journal of Molecular Liquids*, 367(1), 120390.
12. Pinargote, S.N.W.; Smirnov, A.; Peretyagin, N.; Seleznev, A.; and Peretyagin, P. (2020). Direct ink writing technology (3D printing) of graphene-based ceramic nanocomposites: a review. *Nanomaterials*, 10(7), 1300.
13. Siacor, F.D.C.; Chen, Q.; Zhao, J.Y.; Han, L.; Valino, A.D.; Taboada, E.B.; Caldona, E.B.; and Advincula, R.C. (2021). On the additive manufacturing (3D printing) of viscoelastic materials and flow behavior: from composites to food manufacturing. *Additive Manufacturing*, 45(1), 102043.
14. Ordoñez, E.; Gallego, J.M.; and Colorado, H.A. (2019). 3D printing via the direct ink writing technique of ceramic pastes from typical formulations used in traditional ceramics industry. *Applied Clay Science*, 182(1), 105285.
15. Tubío, C.R.; Rama, A.; Gómez, M.; Río, F.; Guitián, F.; and Gil, A. (2018). 3D-printed graphene-Al_2O_3 composites with complex mesoscale architecture. *Ceramics International*, 44(5), 5760-5767.
16. Secor, E.B.; Ahn, B.Y.; Gao, T.Z.; Lewis, J.A.; and Hersam, M.C. (2015). Rapid and versatile photonic annealing of graphene inks for flexible printed electronics. *Advanced Materials*, 27(42), 6683-6688.
17. Naficy, S.; Jalili, R.; Aboutalebi, S.H.; Gorkin, R.A.; Konstantinov, K.; Innis, P.C.; Spinks, G.M.; Poulin, P.; and Wallace, G.G. (2014). Graphene oxide dispersions: tuning rheology to enable fabrication. *Materials Horizons*, 1(3), 326-331.
18. Li, Q.; Dong, Q.; Wang, J.; Xue, Z.; Li, J.; Yu, M.; Zhang, T.; Wan, Y.; and Sun, H. (2022). Direct ink writing (DIW) of graphene aerogel composite electrode for vanadium redox flow battery. *Journal of Power Sources*, 542(1), 231810.
19. Tran, T.S.; Balu, R.; Mata, J.; Dutta, N.K.; and Choudhury, N.R. (2023). 3D printed graphene aerogels using conductive nanofibrillar network formulation. *Nano Trends*, 2(1), 100011.
20. Sun, Q.; Liu, J.; Cheng, H.; Mou, Y.; Liu, J.; Peng, Y.; and Chen, M. (2019). Fabrication of 3D structures via direct ink writing of kaolin/graphene oxide composite suspensions at ambient temperature. *Ceramics International*, 45(15), 18972-18979.
21. Nugroho, W.T.; Dong, Y.; Pramanik, A.; Leng, J.; and Ramakrishna, S. (2021). Smart polyurethane composites for 3D or 4D printing: general-purpose use, sustainability and shape memory effect. *Composites Part B: Engineering*, 223(1), 109104.
22. Duran, M.M.; Moro, G.; Zhang, Y.; and Islam, A. (2023). 3D printing of silicone and polyurethane elastomers for medical device application: a review. *Advances in Industrial and Manufacturing Engineering*, 7(1), 100125.
23. Pandey, H.; Mohol, S.S.; and Kandi, R. (2022). 4D printing of tracheal scaffold using shape-memory polymer composite. *Materials Letters*, 329(1), 133238.

24. Chen, K.; Kuang, X.; Li, V.; Kang, G.; and Qi, H.J. (2018). Fabrication of tough epoxy with shape memory effects by UV-assisted direct-ink write printing. *Soft Matter*, 14(10), 1879-1886.
25. Kuang, X.; Chen, K.; Dunn, C.K.; Wu, J.; Li, V.C.F.; and Qi, H.J. (2018). 3D printing of highly stretchable, shape-memory, and self-healing elastomer toward novel 4D printing. *ACS Applied Materials & Interfaces*, 10(8), 7381-7388.
26. Zhao, W.; Zhang, F.; Leng, J.; and Liu, Y. (2019). Personalized 4D printing of bioinspired tracheal scaffold concept based on magnetic stimulated shape memory composites. *Composites Science and Technology*, 184(1), 107866.
27. Wang, F.; Jiang, M.; Pan, Y.; Lu, Y.; Xu, W.; and Zhou, Y. (2023). 3D Printing photo-induced lignin nanotubes/polyurethane shape memory composite. *Polymer Testing*, 119(1), 107934.
28. Baniasadi, H.; Ajdary, R.; Trifol, J.; Rojas, O.J.; and Seppälä, J. (2021). Direct ink writing of aloe vera/cellulose nanofibrils bio-hydrogels. *Carbohydrate Polymers*, 266(1), 118114.
29. Ge, Q.; Chen, Z.; Cheng, J.; Zhang, B.; Zhang, Y.F.; Li, H.; He, X.; Yuan, C.; Liu, J.; Magdassi, S.; and Qu, S. (2021). 3D printing of highly stretchable hydrogel with diverse UV curable polymers. *Science Advances*, 7(2), 1-10.
30. Malekmohammadi, S.; Sedghi, A.N.; Sabzi, A.; Zarebkohan, A.; Razavi, M.; Vosough, M.; Bodaghi, M.; and Maleki, H. (2021). Smart and biomimetic 3D and 4D printed composite hydrogels: opportunities for different biomedical applications. *Biomedicines*, 9(11), 1537.
31. Zhang, L.; Lee, W.; Li, X.; Jiang, Y.; Fang, N.X.; Dai, G.; and Liu, Y. (2022). 3D direct printing of mechanical and biocompatible hydrogel meta-structures. *Bioactive Materials*, 10(1), 48-55.
32. Chen, Z.; Zhao, D.; Liu, B.; Nian, G.; Li, X.; Yin, J.; Qu, S.; and Yang, W. (2019). 3D printing of multifunctional hydrogels. *Advanced Functional Materials*, 29(20), 1900971.
33. Imrie, P.; Diegel, O.; and Jin, J. (2023). Direct-ink-write 3D printing of "living" polymer hydrogels via type I photoinitiated RAFT polymerization. *Polymer*, 276(1), 125944.
34. Cesarano, J.; Segalman, R.; and Calvert, P.D. (1998). Robocasting provides moldless fabrication from slurry deposition. *Ceramic Industry*, 148(1).
35. Ghazanfari, A.; Li, W.; Leu, M.; Watts, J.; and Hilmas, G. (2017). Mechanical characterization of parts produced by ceramic on-demand extrusion process. *International Journal of Applied Ceramic Technology*, 14(3), 486-494.
36. Liu, N.; Sun, X.; Chen, Z.; Xu, Z.; Dai, N.; Shi, G.; Cai, S.; Lv, X.; and Zheng, C. (2022). Direct ink writing of dense alumina ceramics prepared by rapid sintering. *Ceramics International*, 48(20), 30767-30778.
37. Baltazar, J.; Alves, M.F.R.P.; Santos, C.; and Olhero, S. (2022). Reactive sintering of Al_2O_3–$Y_3Al_5O_{12}$ ceramic composites obtained by direct ink writing. *Ceramics*, 5(1), 1-12.
38. Hossain, S.S.; Son, H.J.; Park, S.; and Bae, C.J. (2023). Extrusion-based 3D printing alumina-silica inks: adjusting rheology and sinterability incorporating waste derived nanoparticles. *Journal of the European Ceramic Society*, 43(11), 4865-4876.

39. Yu, T.; Zhang, Z.; Liu, Q.; Kuliiev, R.; Orlovskaya, N.; and Wu, D. (2020). Extrusion-based additive manufacturing of yttria-partially-stabilized zirconia ceramics. *Ceramics International*, 46(4), 5020-5027.
40. Ebert, J.; Özkol, E.; Zeichner, A.; Uibel, K.; Weiss, Ö.; Koops, U.; Telle, R.; and Fischer, H. (2009). Direct inkjet printing of dental prostheses made of zirconia. *Journal of Dental Research*, 88(7), 673-676.
41. Rodrigues, I.; Guedes, M.; Olhero, S.; Chefdor, A.; Branco, A.C.; Leite, M.; Serro, A.P.; and Figueiredo-Pina, C.G. (2020). Development of free binder zirconia-based pastes for the production of dental pieces by robocasting. *Journal of Manufacturing Processes*, 57(1), 1-9.
42. Teegen, I.S.; Schadte, P.; Wille, S.; Adelung, R.; Siebert, L.; and Kern, M. (2023). Comparison of properties and cost efficiency of zirconia processed by DIW printing, casting and CAD/CAM-milling. *Dental Materials*, 39(7), 669-676.
43. Xu, K. (2014). Electrolytes and interphases in Li-ion batteries and beyond. *Chemical Reviews*, 114(23), 11503-11618.
44. Cheng, M.; Ramasubramanian, A.; Rasul, M.G.; Jiang, Y.; Yuan, Y.; Foroozan, T.; Deivanayagam, R.; Tamadoni, S.M.; Rojaee, R.; Song, B.; Yurkiv, V.R.; Pan, Y.; Mashayek, F.; and Shahbazian-Yassar, R. (2021). Direct ink writing of polymer composite electrolytes with enhanced thermal conductivities. *Advanced Functional Materials*, 31(4), 2006683.
45. Plog, J.; Wang, X.; Lichade, K.M.; Pan, Y.; and Yarin, A.L. (2023). Extremely-fast electrostatically-assisted direct ink writing of 2D, 2.5D and 3D functional traces of conducting polymer Poly(3,4-ethylenedioxythiophene) polystyrene sulfonate- polyethylene oxide (PEDOT:PSS-PEO). *Journal of Colloid and Interface Science*, 651(1), 1043-1053.
46. Liu, H.; Mei, D.; Yu, S.; Qian, S.; and Wang, Y. (2023). Direct ink writing of chopped carbon fibers reinforced polymer-derived SiC composites with low shrinkage and high strength. *Journal of the European Ceramic Society*, 43(2), 235-244.
47. Abas, M.; and Rahman, K. (2016). Fabrication of flex sensors through direct ink write technique and its electrical characterization. *Applied Physics A*, 122(11), 972.
48. Vatani, M.; Engeberg, E.D.; and Choi, J.W. (2015). Conformal direct-print of piezoresistive polymer/nanocomposites for compliant multi-layer tactile sensors. *Additive Manufacturing*, 7(1), 73-82.
49. Parekh, D.P.; Ladd, C.; Panich, L.; Moussa, K.; and Dickey, M.D. (2016). 3D printing of liquid metals as fugitive inks for fabrication of 3D microfluidic channels. *Lab on a Chip*, 16(10), 1812-1820.
50. Li, B.; Clark, P.A.; and Church, K.H. (2007). Robust direct-write dispensing tool and solutions for micro/meso-scale manufacturing and packaging. *International Manufacturing Science and Engineering Conference*, Atlanta, Georgia, USA, 715-721.
51. Markl, M.; and Körner, C. (2016). Multiscale modeling of powder bed–based additive manufacturing. *Annual Review of Materials Research*, 46(1), 93-123.

52. Chen, J.; Xu, L.; Yang, M.; Chen, X.; Chen, X.; and Hong, W. (2019). Highly stretchable photonic crystal hydrogels for a sensitive mechanochromic sensor and direct ink writing. *Chemistry of Materials*, 31(21), 8918-8926.
53. Alam, A.; Saeed, G.; Kim, K.W.; Kim, J.K.; Park, H.S.; and Lim, S. (2023). Direct ink writing (DIW) printed high-performance asymmetric supercapacitor based on 0D@2D silver-nanoparticles@MXene as anode and 0D@2D MnO_2-nanoparticles@MXene as cathode materials. *Journal of Energy Storage*, 72(1), 108227.
54. Bae, J.; Oh, S.; Lee, B.; Lee, C.H.; Chung, J.; Kim, J.; Jo, S.; Seo, S.; Lim, J.; and Chung, S. (2023). High-performance, printable quasi-solid-state electrolytes toward all 3D direct ink writing of shape-versatile Li-ion batteries. *Energy Storage Materials*, 57(1), 277-288.
55. Pesode, P.; Barve, S.; Wankhede, S.V.; and Ahmad, A. (2023). Sustainable materials and technologies for biomedical applications. *Advances in Materials Science and Engineering*, 2023(1), 6682892.
56. Vaiani, L.; Boccaccio, A.; Uva, A.E.; Palumbo, G.; Piccininni, A.; Guglielmi, P.; Cantore, S.; Santacroce, L.; Charitos, I.A.; and Ballini, A. (2023). Ceramic materials for biomedical applications: an overview on properties and fabrication processes. *Journal of Functional Biomaterials*, 14(3), 146.
57. Visscher, D.O.; Bos, E.J.; Peeters, M.; Kuzmin, N.V.; Groot, M.L.; Helder, M.N.; and Zuijlen, P.P. (2016). Cartilage tissue engineering: preventing tissue scaffold contraction using a 3D-printed polymeric cage. *Tissue Engineering Part C: Methods*, 22(6), 573-584.
58. Yan, Y.; Xiong, Z.; Hu, Y.; Wang, S.; Zhang, R.; and Zhang, C. (2003). Layered manufacturing of tissue engineering scaffolds via multi-nozzle deposition. *Materials Letters*, 57(18), 2623-2628.
59. Stanciuc, A.M.; Sprecher, C.M.; Adrien, J.; Roiban, L.I.; Alini, M.; Gremillard, L.; and Peroglio, M. (2018). Robocast zirconia-toughened alumina scaffolds: processing, structural characterisation and interaction with human primary osteoblasts. *Journal of the European Ceramic Society*, 38(3), 845-853.
60. Ashwin, A.J.; and Jafferson, J.M. (2021). State of the art direct ink writing (DIW) and experimental trial on DIW of HAp bio-ceramics. *Materials Today: Proceedings*, 46(1), 1298-1307.
61. Lamnini, S.; Elsayed, H.; Lakhdar, Y.; Baino, F.; Smeacetto, F.; and Bernardo, E. (2022). Robocasting of advanced ceramics: ink optimization and protocol to predict the printing parameters - a review. *Heliyon*, 8(9), e10651.
62. Ramesh, S.; Sara Lee, K.Y.; and Tan, C.Y. (2018). A review on the hydrothermal ageing behaviour of Y-TZP ceramics. *Ceramics International*, 44(17), 20620-20634.
63. Michna, S.; Wu, W.; and Lewis, J.A. (2005). Concentrated hydroxyapatite inks for direct-write assembly of 3-D periodic scaffolds. *Biomaterials*, 26(28), 5632-5639.
64. Li, Y.Y.; Li, L.T.; and Li, B. (2015). Direct write printing of three-dimensional ZrO_2 biological scaffolds. *Materials & Design*, 72(1), 16-20.
65. Cheng, Y.; Chan, K.H.; Wang, X.Q.; Ding, T.; Li, T.; Lu, X.; and Ho, G.W. (2019). Direct-ink-write 3D printing of hydrogels into biomimetic soft robots. *ACS Nano*, 13(11), 13176-13184.

66. Guan, R.; Zheng, H.; Liu, Q.; Ou, K.; Li, D.S.; Fan, J.; Fu, Q.; and Sun, Y. (2022). DIW 3D printing of hybrid magnetorheological materials for application in soft robotic grippers. *Composites Science and Technology*, 223(1), 109409.
67. Wang, Z.; Wu, Y.; Zhu, B.; Chen, Q.; Wang, L.; Zhao, Y.; Sun, D.; Zheng, J.; and Wu, D. (2023). A magnetic soft robot with multimodal sensing capability by multimaterial direct ink writing. *Additive Manufacturing*, 61(1), 103320.
68. Subash, A.; and Kandasubramanian, B. (2020). 4D printing of shape memory polymers. *European Polymer Journal*, 134(1), 109771.
69. Mostafaei, A.; Elliott, A.M.; Barnes, J.E.; Li, F.; Tan, W.; Cramer, C.L.; Nandwana, P.; and Chmielus, M. (2021). Binder jet 3D printing—process parameters, materials, properties, modeling, and challenges. *Progress in Materials Science*, 119(1), 100707.
70. Croom, B.P.; Abbott, A.; Kemp, J.W.; Rueschhoff, L.; Smieska, L.; Woll, A.; Stoupin, S.; and Koerner, H. (2021). Mechanics of nozzle clogging during direct ink writing of fiber-reinforced composites. *Additive Manufacturing*, 37(1), 101701.
71. Hossain, S.S.; and Lu, K. (2023). Recent progress of alumina ceramics by direct ink writing: ink design, printing and post-processing. *Ceramics International*, 49(7), 10199-10212.
72. Roussel, N. (2018). Rheological requirements for printable concretes. *Cement and Concrete Research*, 112(1), 76-85.
73. Owens, J.T.; Das, A.; and Bortner, M.J. (2022). Accelerating heat transfer modeling in material extrusion additive manufacturing: from desktop to big area. *Additive Manufacturing*, 55(1), 102853.